Dimensionless approach of a polymer electrolyte membrane water electrolysis: Advanced analytical modelling

Farid Aubras, Maha Rhandi, Jonathan Deseure, Amangoua Jean-Jacques Kadjo, Miloud Bessafi, Jude Majasan, Brigitte Grondin-Perez, Florence Druart, Jean-Pierre Chabriat

Dimensionless approach of a Polymer Electrolyte Membrane Water Electrolysis: Advanced Analytical Modelling

Farid AUBRAS[a,b], Maha RHANDI[a*], Jonathan DESEURE[a], Amangoua Jean-Jacques KADJO[b], Miloud BESSAFI[b], Jude MAJASAN[c], Brigitte GRONDIN-PEREZ[b], Florence DRUART[a] and Jean-Pierre CHABRIAT[b]

[a] Univ. Grenoble Alpes, Univ. Savoie Mont Blanc, CNRS, Grenoble INP, LEPMI, 38000 Grenoble, France

[b] Univ. De la Réunion, LE2P, 97715 Saint-Denis, France

[c] Electrochemical Innovation Lab, Department of Chemical Engineering, UCL, London, UK

[*] Corresponding author. Tel.: +33 (0) 4 76 82 65 24. E-mail address: maha.rhandi@lepmi.grenoble-inp.fr

Abstract

The water electrolysis appears as a sustainable solution for hydrogen production. The proton exchange membrane electrolyzers (PEM-E) play an increasingly important role in the development of hydrogen technology. Fast analysis of PEM-E efficiency using a mathematical approach is an effective tool for the improvement of these devices. This work presents a closed-form solution of single cell PEM-E modelling. The approach considers charge and mass transport balances. The one-dimensional study focuses on the anodic and the cathodic catalyst layer and the membrane using only dimensionless parameters. The analytical model allows to describe the water management as a function of pressure gradient and current density using a dimensionless ratio of water transport process ($\beta_{m,}$). This model is endorsed by experimental data. Dimensionless parameters like Thiele modulus ($\beta_{a,c}$) or Wagner number ($\omega_{a,c}$) are reached using numerical optimization methods. Changing values of dimensionless

numbers, allow the observation of the impact of the two-phase flow regimes on the electrochemical performances.

Keywords: closed-form solution, dimensionless model, PEM water electrolysis, two-phase flow characterisation

1. Introduction

The contribution of hydrogen to global energy consumption will increase dramatically, to approximately 50% by the end of the 21st century, due to the development of efficient end-use technologies, possibly even becoming the major final energy carrier [1]. Trends and innovations in hydrogen production were recently reviewed [2], [3]. Therefore, water electrolysis for hydrogen production has many advantages, first one is the simple process: only water and electricity are required to produce hydrogen. According to Joshua Mermelstein and Oliver Posdziech [4] an electrochemical device based on solid oxide electrolysis cell can reach an electrical efficiency close to 100% lower heating value (LHV). Moreover, this system could be combined with different strategies of power to gas (e.g. methanation reactor) [5]. However, due to high operating temperatures of these cells, the material stability is affected which decreases the cell performance [6]. The PEM technology is now compatible with fast start-up/shutdown, hence with intermittent operation [7] . Furthermore, the operation at ambient temperature makes it easier to real application. Among the electrolysis technologies, the Proton Exchange Membrane Electrolysis (PEM-E) is the best possible compromise in the current industrial process. PEM-E can electrolyze water with low energetic consumption and directly deliver pressurized hydrogen [8].

PEM-E energy conversion system converts electrical energy into chemical energy. The reactant involved is liquid water and the products are oxygen and hydrogen gas as represented in Equations (1-3) below:

$$\text{Anodic reaction: } H_2O \rightarrow \frac{1}{2}O_2 + 2H^+ + 2e^- \quad (1)$$

$$\text{Cathodic reaction: } 2H^+ + 2e^- \rightarrow H_2 \quad (2)$$

Overall reaction: $H_2O \rightarrow \frac{1}{2}O_2 + H_2$ (3)

Figure 1 : Single cell proton exchange membrane electrolysis (PEM-E)

Fig. 1 shows a schematic representation of a single cell of the Proton Exchange Membrane Electrolysis (PEM-E) [9]. The single cell consists of a proton exchange membrane, two electrodes, and flow field plates having flow channels machined in them, through which electrical energy is supplied to the electrodes. The flow channels are required to achieve circulation of the reactant (H_2O at the anode side) and products (O_2 at the anode side and H_2 at the cathode side). The architecture of PEM-E is similar to proton exchange membrane fuel cells (PEMFC). The water flow at the inlet of the channels is distributed toward the anodic current collector. The protons pass through the membrane from the anode to the cathode and re-associating with the electrons to form gaseous hydrogen. The resulting hydrogen diffuses through the cathodic current collector and toward the outlet of the cathodic distribution channel. Simultaneously, oxygen bubbles are removed from the electrode into the anodic current collector and the water flow sweeps the bubbles away.

As a consequence, the two-phase flow in the anode side is thus critical for PEM-E, The model presented by S. S. Lafmejani et al. [10] is a comprehensive CFD model that comprises multiphase flow in porous media and micro-channel, electro-chemistry in catalyst layers, ion transport in membrane: momentum, mass and charge balances. Moreover, this model can help to investigate the gas–liquid flow impacts on the electrolyzer performance. In addition, the modelling results can be used for improved porous transport layer, catalyst layer and flow field design for water electrolyzer cells. According to A. Nouri-Khorasani et al [11], the wettability of the catalyst proves to be the most influential material property for bubble-flow initiation. Modelling and CFD simulations are powerful tools to understand the bubble flow behavior [12], however the computation time required is not compatible with online analysis of real pattern of electrolysis cell. The best experimental way consists on in-situ neutron imaging [13], [14]. This technic has highlighted that the water management through the membrane plays a critical role in cell performances [15]. In our previous work, a 1D model of a membrane electrode assembly (MEA) has been performed to analyze the cell behavior [16]. However, the computing results of numerical modelling do not provide characteristic parameters to access a faster analysis of experimental data. Closed-form equations and dimensionless number are well adapted to analyze experimental data.

Analytical modelling is a mathematical model that has a closed-form solution. It is the mathematical solution of differential equations representing the internal phenomenology present within a given system as a mathematical analytic function. In additional to this, the dimensionless approach allows to obtain a set of dimensionless mathematical equations. Where the dimensionless numbers are representative of physical phenomena. In the case of PEM-E, the limiting phenomena will be:

- Proton diffusion in the membrane and the catalytic layer
- The diffusion of water in the membrane
- Electrochemical kinetics at catalytic layers
- Electro-osmotic transport in the membrane
- Osmotic pressure transport in the membrane

The dimensionless approach is used to discuss mean values and spatial distributions of current densities, over potential, water contents and membrane resistance. In the literature, studies on the analytical modelling approaches have essentially focused on fuel cells.

Jeng et al. [17] proposed an analytical resolution of mass transport, electrochemical kinetics and charge balance at the catalytic layer and the cathodic diffusion layer. Nevertheless, the work provides no information concerning the mass transport inside the membrane as well as on its state of hydration. These authors exhibit a phenomenological approach based on dimensionless numbers.

Gyenge [18] proposed an original study of the dimensionless numbers present at the MEA of a PEM fuel cell by means of the Quraishi-fahidy method [19]. Experimentally validated, the model makes it possible to obtain spatial quantities such as water content, over potentials and current densities. Another interesting aspect of this study is the array of dimensionless numbers specific to fuel cells including the Wagner number [20] and the number of Damkholer [21]. These dimensionless numbers will be presented in this study.

Current literature suggests that the analytical modelling and dimensionless methods are currently underutilized in fuel cell (PEMFC) and electrolysis (PEM-E) domain. Therefore, this work presents an innovative analytic approach to quantify electrochemical performances based on the dimensionless methodology.

This work presents an analytical dimensionless modelling of single cell proton exchange membrane water electrolysis (PEM-E) at low temperature with a focus on the Membrane Electrode Assembly (MEA). An analytical solution of the differential equations representing the processes occurring in the catalyst layers and membrane are established to quantify distributions and average values of water content and current densities. This method makes it possible to obtain dimensionless numbers that are operational and intrinsic to the PEM-E system. Dimensionless analysis provided an original approach to describe water management through the membrane and catalyst use inside the catalyst layer. Moreover, these numbers are used to characterize the single cell throughout the polarization curves and to allow quantifying the influence of two-phase flow regimes on the electrochemical performances.

2. Model description

The model is based on reported studies in the literature on the dimensionless modelling of the MEA of a fuel cell [18][17]. However, the dimensionless approach of pressurized PEM-E has not yet been proposed. In our previous work [16] we have evidenced three apparent two-phase flow regimes: a non-coalesced bubble regime (NCB regime) for small current densities, a coalesced bubble regime (CB regime) for average current densities and a bullous blockage regime called the "slug flow regime" for high current densities. The boundary conditions of this 1D model depends on two-phase flow regimes.

Figure 2: One dimensional schematic representation of PEM-E with $\delta_{a,c,m}$ are the common PEM assembly thicknesses

Fig. 2 shows the geometry and the dimensionless current density boundary conditions used in this study. While the diffusion layer is completely saturated with water, only the catalytic layers and the membrane are represented. However, this assumption is well assumed for cathodic side of PEM-E.

It is well known that the analytical solution of the differential equations assumes a linear equation set to attain analytical solutions. As part of a first analytic approach, the diffusion layers, the catalytic layers and the membrane are considered to be isothermal. The water content gradient is neglected in the catalytic layer. In this approach, the anodic catalytic layer is completely saturated with water. Therefore, no mass balance is performed, and it is assumed that $\lambda_{a,c}$ is equal to a constant in the catalytic layers.

Where, $\lambda_{a,c,m}$ is the dimensionless water content of protonic electrolyte polymer in anode, cathode and membrane.

The assumptions considered are:

- The steady state $\frac{d}{dt} = 0$
- The isothermal system
- The protonic conductivity occurs the main part of ohmic drop
- The diffusion and the anodic reaction layers are completely saturated in water

- The protonic current at the anodic diffusion layer and cathodic diffusion layer is nil

This phenomenological description is based on mass balance in the membrane, a charge balance in the MEA and electrochemical kinetics at the catalytic layers assuming one dimensional approach as shown in Figure 2.

2.1. Electrochemical equation

- At the anode

Butler-Volmer's law describes electrochemical kinetics at the electrode [22] [23]. However, when PEM-E operates at high current density (quite far from the equilibrium potential $E_{eq}^{a,c}$(V) it is possible to simplify the Butler Volmer's law in Tafel's law and describes the steady state charge balance as follows:

$$\frac{di_a}{dx} = \frac{\gamma_a}{\delta_a} i_{0,a} e^{\frac{\alpha_a F \eta_a}{RT}} \qquad (4)$$

Where, $i_{0,a}$ denotes the current exchange density (A.m^{-2}), $\gamma_{a,c}$ roughness factor (m^2.m^{-2}), $\alpha_{a,c}$ the anodic and cathodic exchange coefficients (-), R gas constant (J.mol^{-1}.K^{-1}), F the Faraday constant (C.mol^{-1}), T temperature (K), $\delta_{a,c,m}$ layer thicknesses of the anodic, cathodic catalytic layer and membrane (m), $\eta_{a,c,m}$ the overpotential at anode, cathode and membrane (V), $i_{a,c,m}$ the current density through the anode, cathode and membrane (A.m^{-2}) and x the axis of the system (m).

The catalytic layer consists of an ionic phase and an electric phase. The over potential at the catalytic layer is the difference between the ionic potential Φ_{ionic} (V) and the electric potential Φ_{elec} (V) and equilibrium potential $E_{eq}^{a,c}$ (V). On the other hand, as stated in the assumptions, the protonic conductivity is very low compared to the electrical conductivity [24]. Therefore, the over potential is calculated using only the ionic potential Φ_{ionic} given by Ohm's law as:

$$\nabla\eta_a = -\nabla\Phi_{ionic} = -\frac{i_a}{\sigma^{eff}_{H^+,a}} \quad (5)$$

Where $\sigma^{eff}_{H^+,a,c,m}$ is the effective protonic conductivity (S.m) of the Nafion® phase in anode, cathode and membrane. The proton conductivity is obtained using the Neubrand model [25][21]:

Deriving the Equation (4) and using the Equation (5) a nonlinear second order differential equation, involving the current density at the reaction layer i_a can be obtained (Eq. 6):

$$i''_a = \frac{\alpha_a F}{RT\sigma^{eff}_{H^+,a}} i'_a i_a \quad (6)$$

- At the cathode

As it has been done for the anodic catalytic layer, the electrochemical kinetics at the cathode is obtained by Tafel's law. Using the similar development as the anode side, the differential equation of the electrochemical kinetics of the cathodic current density at the reaction layer is written as follows:

$$i''_c = \frac{\alpha_c F}{RT\sigma^{eff}_{H^+,c}} i'_c i_c \quad (7)$$

- In the membrane

The membrane is electrically isolated. Only protons can pass through the membrane from the anodic side to the cathodic side. The current density through the membrane is constant and equal to the operating current density J_0. The distribution of the over potential is written using charge balance (Eq. 8):

$$\frac{\mathrm{d}\eta_m}{\mathrm{dx}} = -\frac{J_0}{\sigma^{eff}_{H^+,m}} = -K_m \quad (8)$$

Where J_0 is the operating current density ($A.m^{-2}$)

2.2. Mass balance

- At the hydrated anode

As stated in the assumptions of the model, the diffusion and the reaction anodic layers are saturated with water, thus the water content at these layers is constant and equal to saturation water content $\lambda_{a,c,m}^{sat}$. The water content at the anode depends on the operating conditions such as the operating current density J_0 and the topological parameters of the membrane. According to experimental work [16], at the catalytic layer/diffusion layer interface, the saturation water content appears as a function of the operating bubbly flow regime in the cathodic channel side. Indeed, we have observed two possible values:

$$\lambda_a = \lambda_a^{sat,liq} = 22 \; or \; \lambda_a = \lambda_a^{sat,vap} = 18 \quad (9)$$

Certainly, it is possible that weak temperature gradients in catalyst layer involves a non-equilibrium condition in catalyst layer because the cooling effect of water flux during electrolysis is clogged by thin bubbles like a thin gas film. Therefore, large bubbles can provide fresh water to catalyst layer: two apparent saturated values are possible 18 for vapor condition and 22 for liquid condition.

- At the cathode

In the case of a hydrated cathode, the diffusion layer and the reaction layer have a homogeneous water distribution. In our simulations, to investigate the entire experimental measurements, both values are used:

$$\lambda_c = \lambda_c^{sat,liq} = 22 \; or \; \lambda_c = \lambda_c^{sat,vap} = 18 \qquad (10)$$

- In the membrane

The water mass balance is defined using the steady-state mass balance:

$$D_{H_2O} \Delta c_{H_2O} = \vec{v}_m . \vec{\nabla} c_{H_2O} \quad (11)$$

Where c_{H_2O} is the bulk concentration of water (mol.m^{-3}) in the membrane and the flux, where $\vec{v}_m$ is the water velocity (m.s^{-1}) inside the membrane and D_{H_2O} is the diffusion coefficient of water in the membrane (m^2.s^{-1}).

Schlögl's equation of motion describes the convective term of the mass-transfer; electric potential and pressure gradients generate convection within the pores of the ion-exchange membrane (Bernardi & Verbrugge 1991)[26]:

$$\vec{v}_m = \frac{\kappa_\Phi}{\mu} z_f c_f F \vec{\nabla}\Phi - \frac{\kappa_p}{\mu}\vec{\nabla}p \qquad (12)$$

Where μ denotes the water viscosity (kg.m^{-1}.s^{-1}), κ_Φ is the electro-kinetic permeability (m^2), z_f is the fixed-charge number in the membrane, c_f is the fixed-charge concentration (mol.cm^{-3}) and κ_p is the hydraulic permeability (m^2).

Water molecules that are transported through the PEM from the anode to the cathode along with protons (H^+) will be referred to as water content λ_m transport in the PEM, where λ_m is the dimensionless quantity defined as follows [27]:

$$\lambda_m = \frac{EWV_{ex}c_{H_2O}}{\rho_{dry}^m} \leftrightarrow c_{H_2O} = \frac{\rho_{dry}^m \lambda_m}{EWV_{ex}} \qquad (13)$$

Where ρ_{dry}^m (kg.m^{-3}) is the dry density of the PEM, EW is the equivalent weight (mass) of the PEM (kg.mol^{-1}), c_{H_2O} is the water concentration (mol.m^{-3}) and V_{ex} is the coefficient of expansion of the PEM.

The water mass balance can be written as follows:

$$D_{H_2O}\Delta\lambda_m = -\frac{\kappa_\Phi}{\mu} z_f c_f F \frac{\vec{J}}{\sigma^m}.\vec{\nabla}\lambda_m - \frac{\kappa_p}{\mu}\vec{\nabla}p.\vec{\nabla}\lambda_m \qquad (14)$$

With the upper value of λ_m is $\lambda_m^{sat,liq} = 22$

3. Dimensionless approach

The main objective is to obtain a set of differential equations using dimensionless numbers. In order to achieve this aim, a dimensionless method should be introduced using dimensionless parameters gathered in the table 1.

Table 1: Dimensionless parameters

Dimensionless current density	$i^*_{a,c,m} = \frac{i_{a,c,m}}{J_0}$
Dimensionless activation over potential	$\eta^*_{a,c} = \frac{\eta_{a,c}}{\frac{RT}{\alpha_{a,c}F}}$
Dimensionless ohmic voltage drop	$\eta^*_m = \frac{\eta_m}{\frac{RT}{F}}$
Dimensionless thickness	$x^*_{a,c,m} = \frac{x_{a,c,m}}{\delta_{a,c,m}}$
Dimensionless water content	$\lambda^*_m = \frac{\lambda_m}{\lambda_m^{sat,liq}}$

3.1. Dimensionless electrochemical approach

- At the anode

Considering the differential equation (6) and the dimensionless variables (Table 1), the dimensionless current density i^*_a is governed by the following differential equation:

$$i^{*\prime\prime}_a = \beta_a i^{*\prime}_a i^*_a \qquad where \;\; \beta_a = \frac{J_0 \delta_a F}{RT\sigma^{eff}_{H^+,a}} \quad (15)$$

The dimensionless over potential is obtained by Tafel's law (1):

$$i^{*\prime}_a = \zeta_a \exp(\eta^*_a) \quad where \;\; \zeta_a = \frac{\gamma_a}{J_0} i_{0,a} \quad (16)$$

- At the cathode

The approach is similar at the cathode side:

$$i_c^{*\prime\prime} = \beta_c i_c^{*\prime} i_c^* \qquad where\ \ \beta_c = \frac{J_0 \delta_c F}{RT\sigma_{H^+,a}^{eff}} \quad (17)$$

The dimensionless over potential is:

$$i_c^{*\prime} = -\zeta_c \exp(-\eta_c^*) \quad where\ \ \zeta_c = \frac{\gamma_c}{J_0} i_{0,c} \quad (18)$$

Table 2: Boundary conditions

At the diffusion layer / anodic catalytic layer interface, the protonic current density is nil	$i_a^*(0) = 0$
At the diffusion layer / cathodic catalytic layer interface, the protonic current density is nil	$i_c^*(1) = 0$
A constant current density at the membrane catalyst layer interface equal to the operating current density	$i_a^*(1) = -1$ $i_c^*(0) = 1$

3.2. Dimensionless mass transport in the membrane approach

By associating equation (14) with the dimensionless numbers described by the parameters of (Table 1), the mass transport at the membrane is written as follows:

$$\lambda_m^{*\prime\prime} + \beta_m \lambda_m^{*\prime} = 0 \qquad where\ \ \beta_m = \frac{\delta_m}{D_{H_2O}} \left(\frac{\kappa_\Phi}{\mu} z_f c_f F \frac{J_0}{\sigma^m} + \frac{\kappa_p}{\mu} \nabla p\right) \quad (19)$$

4. Analytical solution

The details of analytical solutions of previously obtained differential equations are available in supplementary materials (details of mathematical contents). These solutions compute the spatial distributions and the averaged values of the current densities, over potential and water content at the membrane.

4.1. Electrochemical approach

4.1.1. Over potential at the catalytic layer

At the anode and the cathode, the limiting processes considered are the electrochemical reactions and the proton resistance of the polymer phase. The coupling of these two phenomena is at the origin of the over potential at the catalytic layers named $\eta_{a,c}^{*}$ obtained previously with the differential equations involving the current density $i_{a,c}$. The analytical solutions are defined by:

At the anode:

$$i_a^* = \frac{1}{K_a^2 \exp\left(-2\sqrt{\beta_a}|K_a^1|x_a^*\right) - \frac{\sqrt{\beta_a}}{2|K_a^1|}} + \frac{|K_a^1|}{\sqrt{\beta_a}} \quad (20)$$

At the cathode:

$$i_c^* = \frac{1}{K_c^2 \exp\left(-2\sqrt{\beta_c}|K_c^1|x_c^*\right) - \frac{\sqrt{\beta_c}}{2|K_c^2|}} + \frac{|K_c^1|}{\sqrt{\beta_c}} \quad (21)$$

With K_a^1, K_a^2, K_c^1 and K_c^2 integration constants.

Equations (13) & (17) can be written as:

$$\eta_a^* = \ln\left(\frac{i_a^{*\prime}}{\zeta_a}\right) = \ln\left(-\frac{\sqrt{\beta_a}K_a^2K_a^1}{\zeta_a}\frac{\exp\left(-2\sqrt{\beta_a}K_a^2x_a^*\right)}{\left(K_a^1\exp\left(-2\sqrt{\beta_a}K_a^2x_a^*\right)-\frac{\sqrt{\beta_a}}{2K_a^2}\right)^2}\right) \quad where\ \zeta_a = \frac{\gamma_a}{J_0}i_{0,a} \quad (22)$$

$$\eta_c^* = -\ln\left(-\frac{i_c^{*\prime}}{\zeta_c}\right) = -\ln\left(-\frac{\sqrt{\beta_c}K_c^2K_c^1}{\zeta_c}\frac{\exp\left(-2\sqrt{\beta_c}K_c^2x_c^*\right)}{\left(K_c^1\exp\left(-2\sqrt{\beta_c}K_c^2x_c^*\right)-\frac{\sqrt{\beta_c}}{2K_c^2}\right)^2}\right) \quad where\ \zeta_c = \frac{\gamma_c}{J_0}i_{0,c} \quad (23)$$

Highlighting the Wagner number ($\omega_{a,c}$):

$$\eta_a^* = \ln\left(-\frac{\beta_a^{\frac{3}{2}} K_a^2 |K_a^1|}{\omega_a} \frac{\exp(-2\sqrt{\beta_a}|K_a^1| x_a^*)}{\left(K_a^2 \exp(-2\sqrt{\beta_a}|K_a^1| x_a^*) - \frac{\sqrt{\beta_a}}{2|K_a^1|}\right)^2} \right) \quad where\ \omega_a = \zeta_a \beta_a = \frac{\gamma_a i_{0,a} \delta_a F}{2RT_a \sigma_a^{H^+}} \quad (24)$$

$$\eta_c^* = -\ln\left(-\frac{\beta_c^{\frac{3}{2}} K_c^2 |K_c^1|}{\omega_c} \frac{\exp(-2\sqrt{\beta_c}|K_c^1| x_c^*)}{\left(K_c^2 \exp(-2\sqrt{\beta_c}|K_c^1| x_c^*) - \frac{\sqrt{\beta_c}}{2|K_c^1|}\right)^2} \right) \quad where\ \omega_C = \zeta_c \beta_c = \frac{\gamma_c i_{0,c} \delta_c F}{2RT_c \sigma_c^{H^+}} \quad (25)$$

The average anodic and cathodic activation over potential are obtained by the relation:

$$\overline{\eta_{a,c}^*} = \int_0^1 \eta_{a,c}^* \, dx_{a,c}^* \quad (26)$$

4.1.2. Over potential through the membrane

The distribution of the dimensionless ohmic drop to the membrane is written as follows:

$$\eta_m^* = -K_m^1 x_m^* + K_m^2 \quad where\ K_m^2 = \eta_{a,int}^* \quad (27)$$

4.1.3. Total over potential

The total dimensionless theoretical over potential of a single cell is the sum of the activation over potential and the ohmic drop:

$$\overline{\eta_t^*} = \overline{\eta_a^*} + \overline{\eta_c^*} + \overline{\eta_{m,}^*} \quad (28)$$

4.2. Mass transport in the membrane

The dimensionless water content distribution to the λ_m^* membrane is the solution to the first-order linear differential equation defined in equation (19). The distribution of water content to the membrane is written as follows:

$$\lambda_m^* = C_1\left(1 + \frac{C_2}{C_1} e^{-\beta_m x_m^*}\right) \quad where \begin{cases} C_1 = \lambda_a{}^* - \frac{\lambda_c{}^* - \lambda_a{}^*}{e^{-\beta_m} - 1} \\ C_2 = \frac{\lambda_c{}^* - \lambda_a{}^*}{e^{-\beta_m} - 1} \end{cases} \quad (29)$$

The dimensionless water content averaged to the membrane is:

$$\overline{\lambda_m^*} = \int_0^1 \lambda_m^* \, dx_m^* = C_1 - \frac{C_2}{\beta_m}\left(e^{-\beta_m} - 1\right) \quad (30)$$

5. Results and discussion

5.1. Dimensionless current density distribution

Figure 3: Dimensionless current density distribution for βa= 0,01 [–•–]; βa= 1 [•]; βa= 5 [– –]; βa= 10 [–] at the room temperature and atmospheric pressure

The Fig. 3 exhibits the current density distribution at the anode side as a function of βa. As βa decreases, the through-plane current density distribution becomes more linear. According to the equation (15) this analytical result shows that the effective protonic conductivity and the operational current density affect the distribution of the current density at the catalyst layer. As a result, the catalyst layer produces more faradic currents throughout the thickness of the catalyst layer at high current density (trivial result) or when ionic conductivity is low in the same way when the ionic conductivity decrease (non-trivial result). Ratio of applied current/effective ionic conductivity drives the performances of anode. The evolution of this ratio can reveal the optimum operating conditions of the anode for a given temperature and catalyst thickness.

5.2. Dimensionless water content distribution

Figure 4: Dimensionless water content distribution at the membrane ((a) full hydrated cathode, (b) full hydrated anode) for βm= 0,1 [–•–]; βm= 1 [– –]; βm= 5 [•]; βm= 10 [–]; βm= -1 [– –]; βm= -5 [•]; βm= -10 [–] at the room temperature and atmospheric pressure

The Fig. 4a and Fig. 4b exhibit the water content distribution at the membrane for different β_m. This analytical result shows that the β_m affects the shape of the water content distribution. According to the equation (19), the β_m represents the diffusion water, the electro-osmotic transport, the protonic conductivity and the flux due to gradient pressure at the membrane. For a $\beta_m \approx 0$, the water content distribution at the membrane is linear accordingly a pure Laplacian equation. Also, the positive or a negative increase of the βm induces a more homogenous water composition through the membrane. Consequently, the ohmic drop can be controlled by the pressure gradient and the cathodic water content e.g. for high cathodic pressure, a full hydrated cathode is needed in order to reduce ohmic drop.

5.3. Dimensionless overpotential variation

Figure 5: (a) Dimensionless anodic overpotential variation with βa (b) Dimensionless cathode overpotential variation with βc at the atmospheric pressure and room temperature for ωa= 1e-5 [–•–]; ωa= 1e-6 [– –]; ωa= 1e-3 [•]; ωa= 1e-4 [–] at the room temperature and atmospheric pressure

The Fig. 5a and Fig. 5b exhibits the polarization curve for various Wagner number at anode and cathode side. These analytical results show that an increase of ω_a improve the electrochemical performance of the PEM-E. According to the equations (24 & 25) a decrease of the electrochemical kinetics or an increase of the protonic conductivity at the catalyst layers involved better electrochemical performance of the PEM-E. This theoretical results is in agreement with the literature [28], which suggest that the topological aspect of the catalyst layers is an important parameters for the optimization of the electrochemical performance of the PEM-E.

5.4. Experimental investigations with analytical dimensionless model

Our model is validated with experimental data of a low pressure electrolyser. The PEM-E single cell used in this study had an active surface area of 8 cm^2, acrylic end plates, titanium pins for cell compression and current supply and platinum-coated titanium is used as the gas diffusion layers. A torque of 1.5 N.m was applied to each of the 8 bolts used to compress the cell. The cell pistons were pneumatically compressed to 20 bar, and deionized water was circulated through both sides from separate storage tanks via a peristaltic pump (Watson Marlow) at the room temperature 20°C. The inlet deionized water was supplied to the anode and cathode compartments by a peristaltic pump at the various flow rates using a recirculation loop with gas removal. The membrane electrode assembly (MEA) used in the cell was obtained from ITM Power. It consisted of two electrodes containing catalysts: 3 $mg.cm^{-2}$ platinum black at the cathode side and 3 $mg.cm^{-2}$ of iridium oxide at the anode side, laminated to either side of a proton conducting solid polymer membrane (Nafion® 117). At the anode (gas diffusion layer) titanium sinter had a thickness equal to 0.35 mm and with 80% of porosity 80 % and at the cathode carbon paper TGP-H-060 with 78% of porosity 78 % and 0.19 mm of thickness was used. The circular membrane has an active surface area of 8 cm^2 and was delivered in dry state.

To obtain optimal performance and minimize resistance, they were activated first ex-situ then in-situ as follows. First, immersion in deionized water at 60 °C for about 18 h then they were left in fresh deionized water for another 2 h at room temperature. Finally, the MEA was conditioned in the cell at a constant current density of 1 $A.cm^{-2}$ for about 18 h (activation process).

Fig.6 exhibits the simulated polarization curve and the experimental data with a flow rate of 200 $ml.min^{-1}$. Only the Wagner numbers $\omega_{a,c}$ at the anode and cathode sides are used as fitting parameters in equation (23). To confirm the validity of this model, a second set of data were compared to the simulation on Fig. 7. This experimental data deals with a pressurized cell from literature experiments of Santarelli et al. [29]. A good agreement is observed between simulations and experiments in both cases. The parametric optimization is achieved using Nelder-Mead Simplex Method algorithm and various tests have been completed to avoid a local minimum. Therefore, this model is a real powerful tool because only two parameters are used to describe the cell efficiency. However, the ionic conductivity of polymeric electrolyte, physical characteristic of membrane and exact thicknesses are required, but no kinetic parameters are required.

Figure 6: Analytical (•) and experimental (–) IV curve with a Nafion® 117 membrane at the atmospheric pressure and room temperature.

Figure 7: Analytical (•) and experimental (–) IV curve with a Nafion® 117 membrane with a pressure of 7 bar at the cathode side and a temperature of 58 °C [29].

Our analytical model can predict the IV curve of the pressurized PEM-E (Fig. 6 & Fig. 7). The Wagner number is the dimensionless key number of our approach. The Wagner number is the ratio between the protonic conductivity and the electrochemical kinetic at the catalyst layer [30][18].

$$\omega_{a,c} = \frac{Electrochemical\ kinetic}{Protonic\ conductivity} \qquad (31)$$

$$\omega_{a,c} = \frac{\gamma_{a,c} i_{0,a,c} \delta_{a,c} F}{2RT_{a,c}\sigma_{a,c}^{H^+}} \qquad (32)$$

In our previous work [16], we have showed that at the anode side two apparent bubbly flow regimes can appear in the PEM-E : for a range of [0-300 A.m^{-2}], there is a non-coalesced bubble regime (NCB regime), for a range of [300-1500 A.m^{-2}], there is a coalesced bubble regime (CB regime) and for a higher value of current density flow regime of two-phase flow in the channel changed from bubbly to slug flow (SF regime) [31]. Here, our main assumption is that the Wagner number can be linked to each different regime of two-phase flow.

According to our previous work for the CB regime, the appearance of larger bubbles increases the free surface at the electrode. The catalyst layer has full access in fresh water and a high protonic conductivity. The Wagner number at anode for the CB regime is constant in CB régime. For the Slug Flow regime >1000 A.m^{-2}, we assume an exponential decrease of the Wagner number at anode. According to H. Ito et al. [31], the transition between bubbly flow (CB) and Slug Flow (SF) is not linear, then we propose the following expression:

$$\omega_a = \omega_{a0}\, e^{(-a(J_0 - J_{trans}))} \qquad (33)$$

At the cathode we assumed that the Wagner number was constant, yet we did not fix the value of ω_c in all range of operating current density. ω_c can take two values, ω_{c1} for $J_0 < J_{trans}$ and ω_{c2} for $J_0 > J_{trans}$. In both experimental sets J_{trans} was close to 100 A.m^{-2}.

Figure 8: Evolution of the Wagner number at the catalyst layer for the anode (a) or for the cathode (b) side function the current density Jo (A.cm^{-2}) at the atmospheric pressure at room temperature (–) and with a pressure of 7 bar at the cathode side at 58 °C (•) (logarithmic scale).

Fig. 8a exhibits the evolution of the anodic Wagner numbers during the electrolysis process. As expected, at high current density, the slug flow regime may clog the channel flow and decrease the active surface area of the MEA [31]. For the slug flow regime, the analytical result shows that the exponential decrease has good agreement with experimental measurements (Fig. 6 and Fig. 7). This decrease is due to the decrease of anode catalyst layer performance. The Wagner number depends on the effective exchange current density (equation (26)). The effective anode exchange current density $(\bar{\gamma}_a . i_{0,a})$ is directly linked to the distribution of specific active area $(\frac{\gamma_a}{\delta_a})$ [25] where, γ_a (called roughness factor) is equal to 0 when the catalytic material is not in contact with reactants [32], accordingly the average coefficient of $\bar{\gamma}_a$ decreases when the slug flow regime block the water in the channel flow.

Surprisingly, Fig. 8b, the Wagner number at cathode was enhanced in the case of pressurized operations when the current density increases. This phenomenon is due to the water management through the membrane (Fig. 4): the water flux is directly linked to oxygen permeation [33] and oxygen affects the catalyst performance of cathode. This phenomenon is more clearly evidenced in the case of pressurized electrolysis.

6. Conclusion

This approach performed on an analytic dimensionless model of PEM-E enables the finding of the three parameters that governed the electrochemical reaction at the catalyst layer and the mass transport through the membrane, namely: The Wagner numbers $\omega_{a,c}$ at the anode and cathode side, a number similar to Thiele modulus at the catalyst layers β_a, and the dimensionless ratio of water transport process through the membrane β_m.

The experimental data exhibited a good agreement with simulations. Moreover, the computations allowed obtaining analytical solutions of the water content in the membrane, the over potential and the current density distribution in the membrane and the catalyst layers. This approach offered a useful tool for the ability of water management through the PEM-E. The dependence of the membrane hydration, total over potential on the Wagner number $\omega_{a,c}$ et β_m was depicted, which can be conveniently referred to when assessing the performance of the PEM-E system.

Exponential reduction of the Wagner numbers at the anode catalyst layer, $\omega_{a,}$ shows the impact of slug flow on cell efficiency at high current density. This result would show that the PEM-E undergo an important decrease of the electrochemical reaction for the high current densities mainly due to gas exhaust. Furthermore, this approach is original and easy to use method that will help with experimental analysis. This closed-form analytic solution of dimensionless model will have many applications for optimization of cell performances:

- the fast computing ability of this dimensionless model will provide large amount of data for hierarchical learning
- the model is adapted to advanced method of process control to model predictive control (MPC)
- this approach can be inserted in a control loop for fault detection methods

References

[1] P. C. K. Vesborg and T. F. Jaramillo, “Addressing the terawatt challenge: scalability in the supply of chemical elements for renewable energy,” *RSC Adv.*, vol. 2, no. 21, p. 7933, 2012, doi: 10.1039/c2ra20839c.

[2] B. Timurkutluk, C. Timurkutluk, M. D. Mat, and Y. Kaplan, “Anode-supported solid oxide fuel cells with ion conductor infiltration,” *Int. J. Energy Res.*, vol. 35, no. 12, pp. 1048–1055, Oct. 2011, doi: 10.1002/er.1832.

[3] J. Chi and H. Yu, “Water electrolysis based on renewable energy for hydrogen production,” *Chin. J. Catal.*, vol. 39, no. 3, pp. 390–394, Mar. 2018, doi: 10.1016/S1872-2067(17)62949-8.

[4] J. Mermelstein and O. Posdziech, “Development and Demonstration of a Novel Reversible SOFC System for Utility and Micro Grid Energy Storage,” *Fuel Cells*, vol. 17, no. 4, pp. 562–570, Aug. 2017, doi: 10.1002/fuce.201600185.

[5] Y. Luo, X. Wu, Y. Shi, A. F. Ghoniem, and N. Cai, “Exergy analysis of an integrated solid oxide electrolysis cell-methanation reactor for renewable energy storage,” *Appl. Energy*, vol. 215, pp. 371–383, Apr. 2018, doi: 10.1016/j.apenergy.2018.02.022.

[6] Y. Yan, Q. Fang, L. Blum, and W. Lehnert, “Performance and degradation of an SOEC stack with different cell components,” *Electrochimica Acta*, vol. 258, pp. 1254–1261, Dec. 2017, doi: 10.1016/j.electacta.2017.11.180.

[7] K. Zeng and D. Zhang, “Recent progress in alkaline water electrolysis for hydrogen production and applications,” *Prog. Energy Combust. Sci.*, vol. 36, no. 3, pp. 307–326, Jun. 2010, doi: 10.1016/j.pecs.2009.11.002.

[8] F. Barbir, “PEM electrolysis for production of hydrogen from renewable energy sources,” *Sol. Energy*, vol. 78, no. 5, pp. 661–669, May 2005, doi: 10.1016/j.solener.2004.09.003.

[9] S. Boulevard *et al.*, “Optimisation d’une Pile A Combustible Réversible: A trois chambres nommée Q-URFC.” 03 2019, [Online]. Available: https://hal.univ-reunion.fr/hal-01953489.

[10] S. S. Lafmejani, A. C. Olesen, and S. K. Kær, “VOF modelling of gas–liquid flow in PEM water electrolysis cell micro-channels,” *Int. J. Hydrog. Energy*, vol. 42, no. 26, pp. 16333–16344, Jun. 2017, doi: 10.1016/j.ijhydene.2017.05.079.

[11] A. Nouri-Khorasani, E. Tabu Ojong, T. Smolinka, and D. P. Wilkinson, “Model of oxygen bubbles and performance impact in the porous transport layer of PEM water electrolysis cells,” *Int. J. Hydrog. Energy*, vol. 42, no. 48, pp. 28665–28680, Nov. 2017, doi: 10.1016/j.ijhydene.2017.09.167.

[12] J. Schillings, O. Doche, M. Tano Retamales, F. Bauer, J. Deseure, and S. Tardu, “Four-way coupled Eulerian–Lagrangian Direct Numerical Simulations in a vertical laminar channel flow,” *Int. J. Multiph. Flow*, vol. 89, pp. 92–107, Mar. 2017, doi: 10.1016/j.ijmultiphaseflow.2016.10.006.

[13] O. Panchenko *et al.*, “In-situ two-phase flow investigation of different porous transport layer

for a polymer electrolyte membrane (PEM) electrolyzer with neutron spectroscopy," *J. Power Sources*, vol. 390, pp. 108–115, Jun. 2018, doi: 10.1016/j.jpowsour.2018.04.044.

[14] F. de Beer, J.-H. van der Merwe, and D. Bessarabov, "PEM Water Electrolysis: Preliminary Investigations Using Neutron Radiography," *Phys. Procedia*, vol. 88, pp. 19–26, 2017, doi: 10.1016/j.phpro.2017.06.002.

[15] O. F. Selamet, U. Pasaogullari, D. Spernjak, D. S. Hussey, D. L. Jacobson, and M. Mat, "In Situ Two-Phase Flow Investigation of Proton Exchange Membrane (PEM) Electrolyzer by Simultaneous Optical and Neutron Imaging," presented at the 220th ECS Meeting, Boston, MA, 2011, pp. 349–362, doi: 10.1149/1.3635568.

[16] F. Aubras *et al.*, "Two-dimensional model of low-pressure PEM electrolyser: Two-phase flow regime, electrochemical modelling and experimental validation," *Int. J. Hydrog. Energy*, vol. 42, no. 42, pp. 26203–26216, Oct. 2017, doi: 10.1016/j.ijhydene.2017.08.211.

[17] K. T. Jeng, C. P. Kuo, and S. F. Lee, "Modeling the catalyst layer of a PEM fuel cell cathode using a dimensionless approach," *J. Power Sources*, vol. 128, no. 2, pp. 145–151, 2004.

[18] E. L. Gyenge, "Dimensionless numbers and correlating equations for the analysis of the membrane-gas diffusion electrode assembly in polymer electrolyte fuel cells," *J. Power Sources*, vol. 152, pp. 105–121, 2005.

[19] M. S. Quraishi and T. Z. Fahidy, "A simplified procedure for dimensional analysis employing si units," *Can. J. Chem. Eng.*, vol. 59, no. 4, pp. 563–566, 1981.

[20] M. Matlosz, C. Creton, C. Clerc, and D. Landolt, "Secondary current distribution in a hull cell boundary element and finite element simulation and experimental verification," *J. Electrochem. Soc.*, vol. 134, no. 12, pp. 3015–3021, 1987.

[21] S. Battersby, P. W. Teixeira, J. Beltramini, M. C. Duke, V. Rudolph, and J. C. D. da Costa, "An analysis of the Peclet and Damkohler numbers for dehydrogenation reactions using molecular sieve silica (MSS) membrane reactors," *Catal. Today*, vol. 116, no. 1, pp. 12–17, 2006.

[22] D. A. Noren and M. A. Hoffman, "Clarifying the Butler–Volmer equation and related approximations for calculating activation losses in solid oxide fuel cell models," *J. Power Sources*, vol. 152, pp. 175–181, 2005.

[23] M. Carmo, D. L. Fritz, J. Mergel, and D. Stolten, "A comprehensive review on PEM water electrolysis," *Int. J. Hydrog. Energy*, vol. 38, no. 12, pp. 4901–4934, 2013.

[24] L. F. L. Oliveira, S. Laref, E. Mayousse, C. Jallut, and A. A. Franco, "A multiscale physical model for the transient analysis of PEM water electrolyzer anodes," *Phys. Chem. Chem. Phys.*, vol. 14, no. 29, pp. 10215–10224, 2012.

[25] J. Ramousse, J. Deseure, O. Lottin, S. Didierjean, and D. Maillet, "Modelling of heat, mass and charge transfer in a {PEMFC} single cell," *J. Power Sources*, vol. 145, no. 2, pp. 416–427, 2005, doi: http://dx.doi.org/10.1016/j.jpowsour.2005.01.067.

[26] D. M. Bernardi and M. W. Verbrugge, "Mathematical model of a gas diffusion electrode bonded to a polymer electrolyte," *AIChE J.*, vol. 37, no. 8, pp. 1151–1163, 1991.

[27] K. M. S. Uddin, L. K. Saha, and N. Oshima, “Water transport through the membrane of PEM,” *Fuel Cell*, vol. 4, pp. 225–238, 2014.

[28] S.-D. Yim *et al.*, “Optimization of PtIr electrocatalyst for PEM URFC,” *Int. J. Hydrog. Energy*, vol. 30, no. 12, pp. 1345–1350, 2005.

[29] M. Santarelli, P. Medina, and M. Calì, “Fitting regression model and experimental validation for a high-pressure PEM electrolyzer,” *Int. J. Hydrog. Energy*, vol. 34, no. 6, pp. 2519–2530, Mar. 2009, doi: 10.1016/j.ijhydene.2008.11.036.

[30] C. Wagner, “Theoretical analysis of the current density distribution in electrolytic cells,” *J. Electrochem. Soc.*, vol. 98, no. 3, pp. 116–128, 1951.

[31] H. Ito *et al.*, “Effect of flow regime of circulating water on a proton exchange membrane electrolyzer,” *Int. J. Hydrog. Energy*, vol. 35, no. 18, pp. 9550–9560, Sep. 2010, doi: 10.1016/j.ijhydene.2010.06.103.

[32] S. J. Lee, S. Mukerjee, J. McBreen, Y. W. Rho, Y. T. Kho, and T. H. Lee, “Effects of Nafion impregnation on performances of PEMFC electrodes,” *Electrochimica Acta*, vol. 43, no. 24, pp. 3693–3701, Aug. 1998, doi: 10.1016/S0013-4686(98)00127-3.

[33] P. Trinke, B. Bensmann, and R. Hanke-Rauschenbach, “Experimental evidence of increasing oxygen crossover with increasing current density during PEM water electrolysis,” *Electrochem. Commun.*, vol. 82, pp. 98–102, Sep. 2017, doi: 10.1016/j.elecom.2017.07.018.

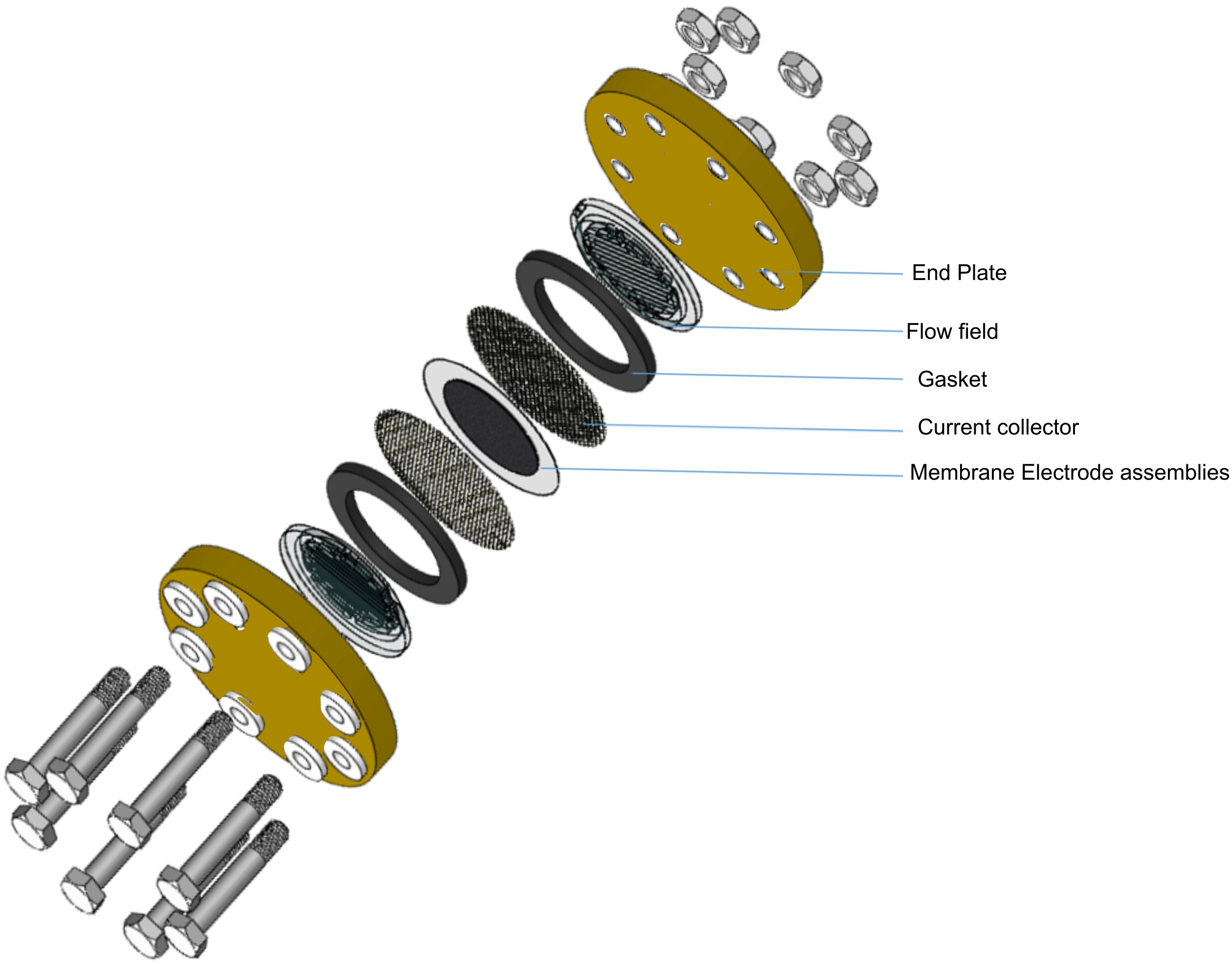

End Plate
Flow field
Gasket
Current collector
Membrane Electrode assemblies

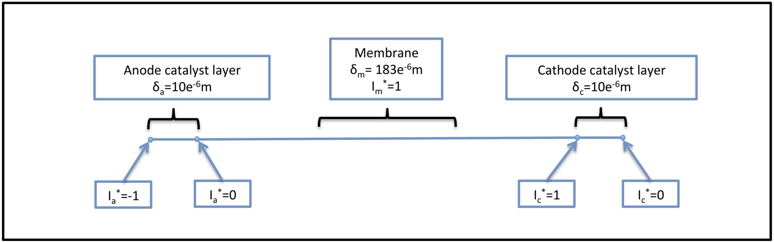

Anode catalyst layer
δ_a=10e^{-6}m
Membrane
δ_m= 183e^{-6}m
I_m^*=1
Cathode catalyst layer
δ_c=10e^{-6}m
I_a^*=-1
I_a^*=0
I_c^*=1
I_c^*=0

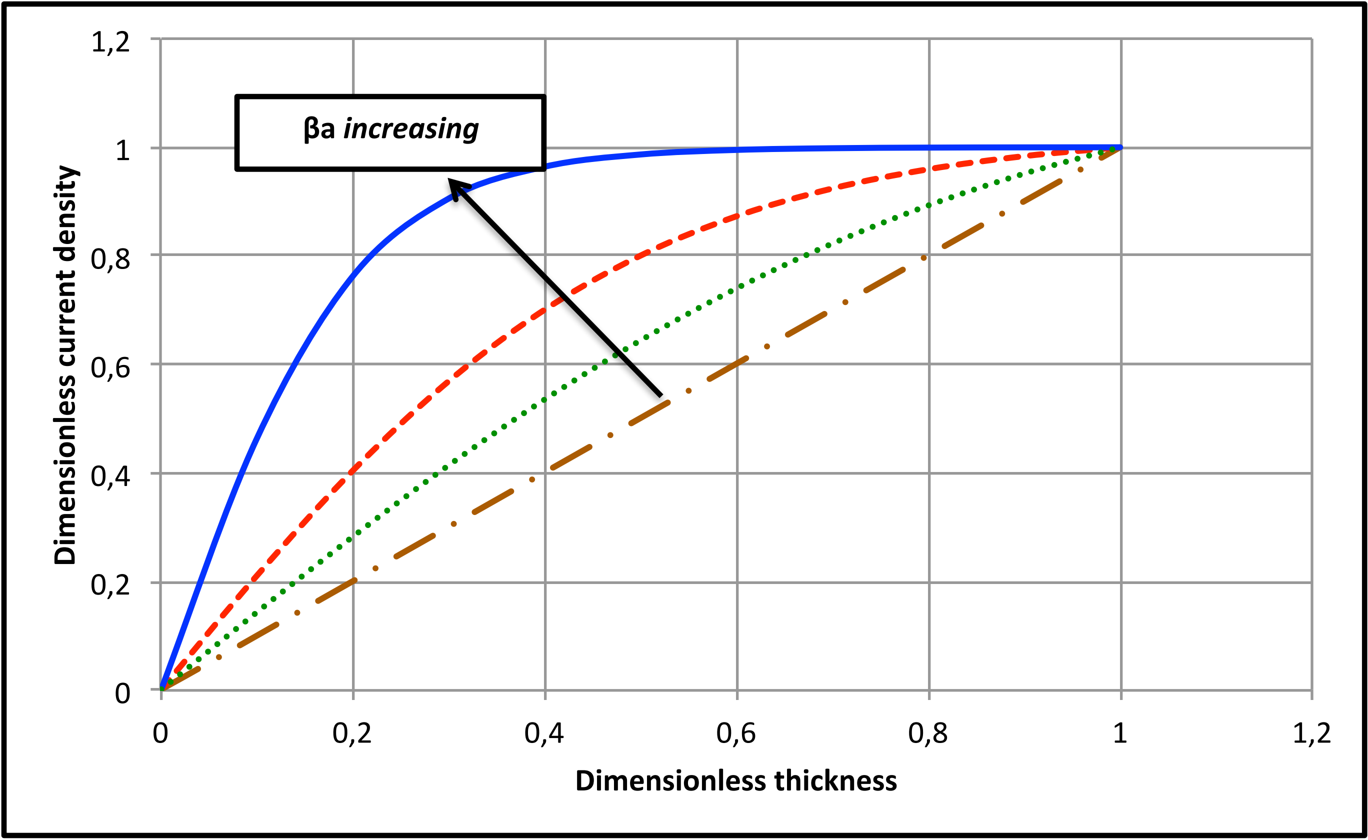

βa *increasing*
Dimensionless current density
Dimensionless thickness
0
0,2
0,4
0,6
0,8
1
1,2

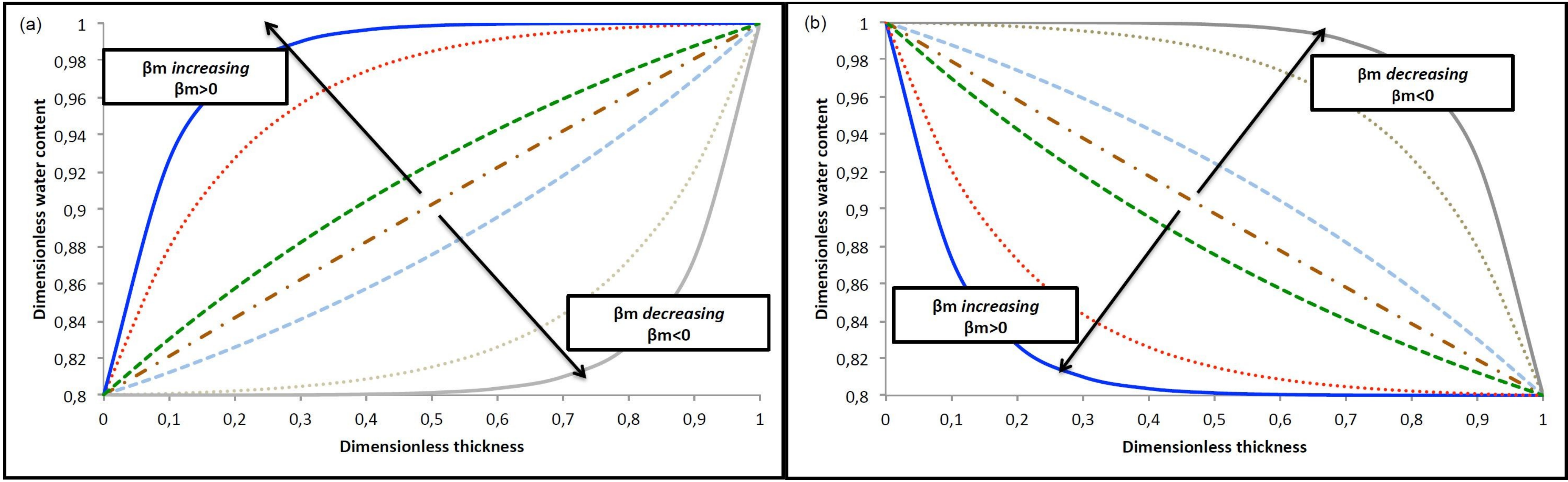

(a)
βm *increasing*
βm>0
βm *decreasing*
βm<0
Dimensionless water content
Dimensionless thickness
(b)
βm *decreasing*
βm<0
βm *increasing*
βm>0
Dimensionless water content
Dimensionless thickness

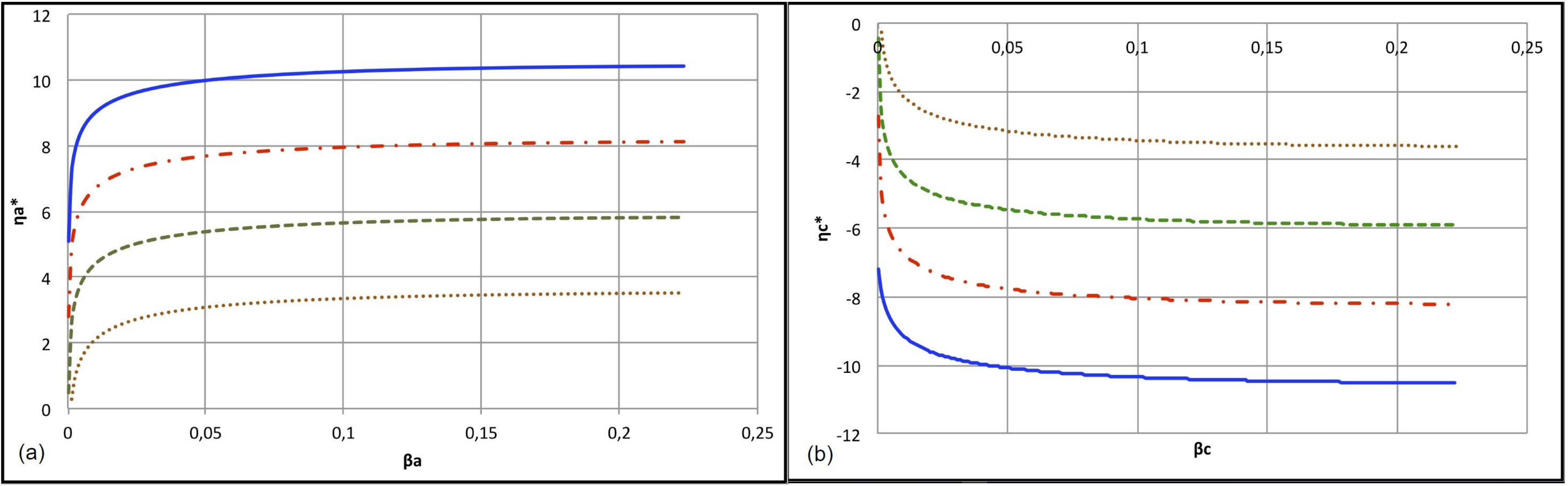
12
10
8
6
4
2
0
ηa*
0
0,05
0,1
0,15
0,2
0,25
βa
(a)
0
-2
-4
-6
-8
-10
-12
ηc*
0
0,05
0,1
0,15
0,2
0,25
βc
(b)

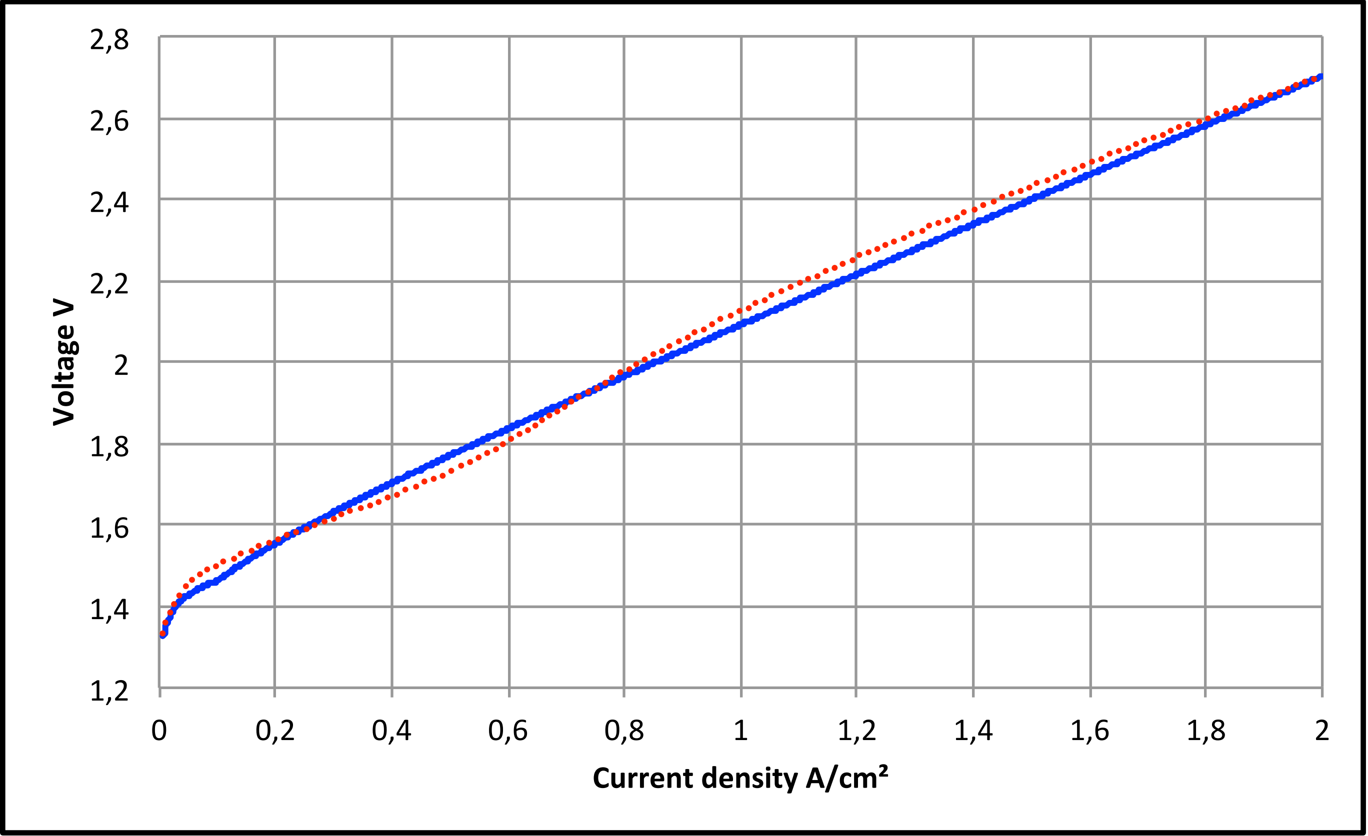

Voltage V
2,8
2,6
2,4
2,2
2
1,8
1,6
1,4
1,2
0
0,2
0,4
0,6
0,8
1
1,2
1,4
1,6
1,8
2
Current density A/cm²

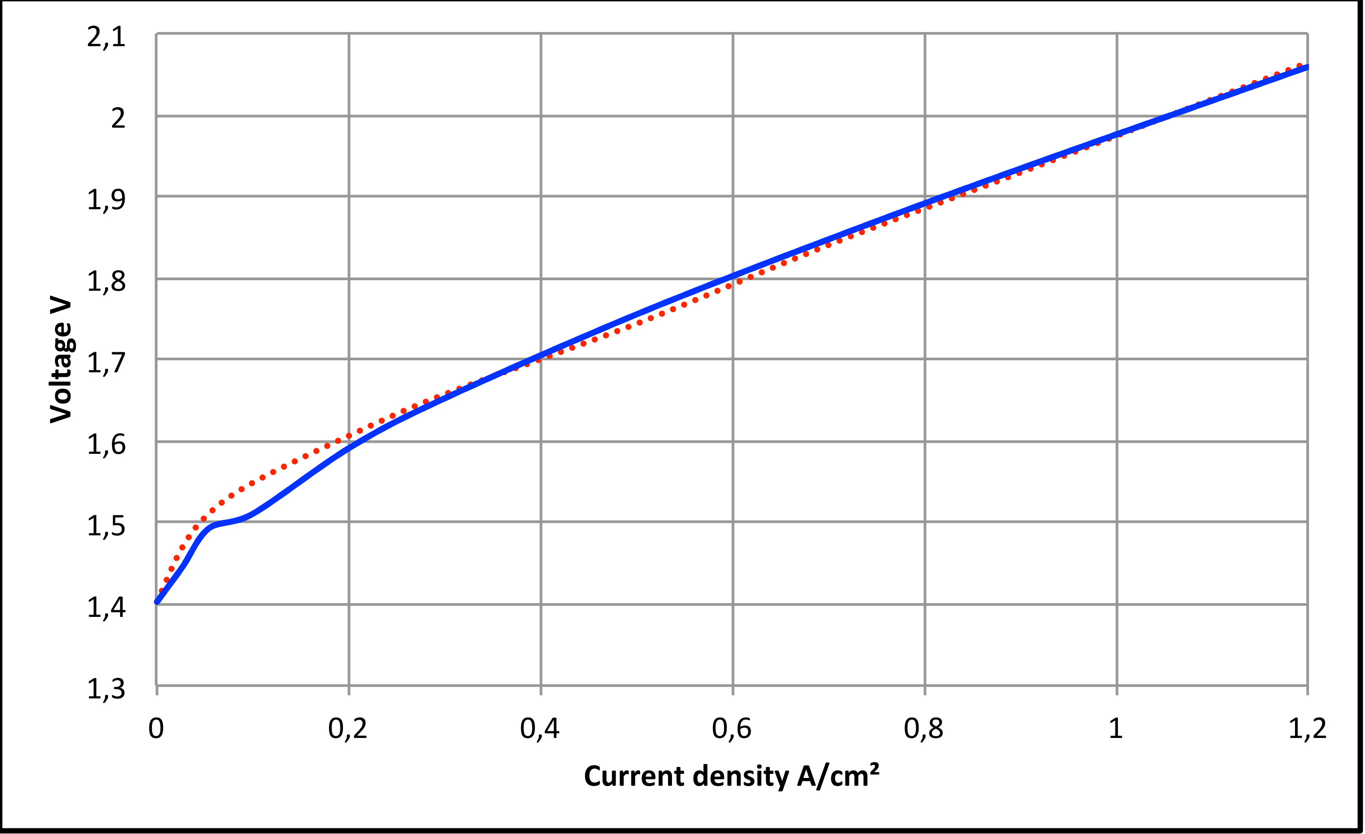
2,1
2
1,9
1,8
1,7
1,6
1,5
1,4
1,3
Voltage V
0
0,2
0,4
0,6
0,8
1
1,2
Current density A/cm²

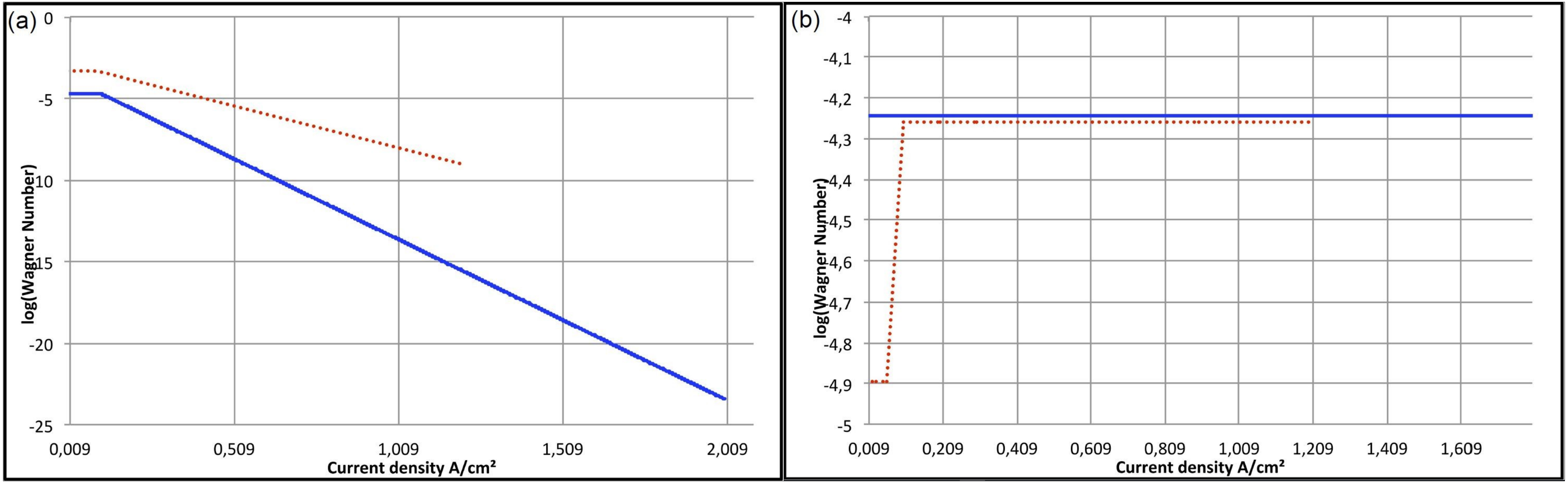

(a)
log(Wagner Number)
0
-5
-10
-15
-20
-25
0,009
0,509
1,009
1,509
2,009
Current density A/cm²
(b)
log(Wagner Number)
-4
-4,1
-4,2
-4,3
-4,4
-4,5
-4,6
-4,7
-4,8
-4,9
-5
0,009
0,209
0,409
0,609
0,809
1,009
1,209
1,409
1,609
Current density A/cm²

Table 1: Dimensionless parameters

Dimensionless current density	$i^*_{a,c,m} = \frac{i_{a,c,m}}{J_0}$
Dimensionless activation over potential	$\eta^*_{a,c} = \frac{\eta_{a,c}}{\frac{RT}{\alpha_{a,c}F}}$
Dimensionless ohmic voltage drop	$\eta^*_{m} = \frac{\eta_{m}}{\frac{RT}{F}}$
Dimensionless thickness	$x^*_{a,c,m} = \frac{x_{a,c,m}}{\delta_{a,c,m}}$
Dimensionless water content	$\lambda^*_{m} = \frac{\lambda_{m}}{\lambda_m^{sat,liq}}$

Table 2: Boundary conditions

At the diffusion layer / anodic catalytic layer interface, the protonic current density is nil	$i_a^*(0) = 0$
At the diffusion layer / cathodic catalytic layer interface, the protonic current density is nil	$i_c^*(1) = 0$
A constant current density at the membrane catalyst layer interface equal to the operating current density	$i_a^*(1) = -1$ $i_c^*(0) = 1$